PAST KNOWLEDGE PEOPLE

ISSN: 2689-1204

Research Article

Journal of Applied Material Science & Engineering Research

Structural, Optical and Electrical Properties of Electron Beam Evaporated Tioxny Films as Selective Solar Absorber Coatings

D Berhane [1,5], M O Rodrigues [5,6], M Henini[5], M Maaza[2,3], A Meldrum[7] and Z Y Nuru[1,2,3*]

[1]*Future Leader –African independent Researcher, Adigrat University, Department of Physics, Adigrat, Ethiopia*

[2]*UNESCO-UNISA Africa Chair, University of South Africa (UNISA), College of Graduate Studies, Muckleneuk ridge, South Africa*

[3]*Nanosciences African Network, iThemba LABS, National Research Foundation, South Africa*

[4]*Aksum University, Department of Physics, Aksum, Ethiopia*

[5]*University of Nottingham, School of Phyiscs and Astronomy, Nottingham NG7 2RD, United Kingdom*

[6]*University of Brasilia, Laboratory of Inorganic and Materials, Asa Norte–Brasil*

[7]*Department of Physics, University of Alberta, Edmonton, Alberta. T6G2E1, Canada*

***Corresponding author**

Z.Y. Nuru, Future Leader –African independent Researcher, Adigrat University, Department of Physics, Adigrat, Ethiopia

Submitted: 29 Jan 2020; **Accepted**: 06 Feb 2020; **Published**: 15 Feb 2020

Abstract

Titanium oxinitride (TiO_xN_y) solar absorber coatings were deposited at different oxygen partial pressures onto Cu, Si and glass substrates using electron beam evaporation technique. XRD diffraction patterns evidenced (111), (200) and (220) orientation of TiN_x phase. The preferred orientation of the films changed with oxygen partial pressure. XPS revealed the intensity of both Ti $2P_{3/2}$ and Ti $2P_{1/2}$ increases as a function of oxygen flow, and also shifted towards higher binding energy, indicating more oxidized state of Ti species than that of TiO_2 due to incorporation of nitrogen atoms. Formation of uniformly distributed spherical like particles and an increase in surface roughness of the TiO_xN_y films were observed as a function of oxygen partial pressure as depicted from SEM and AFM, respectively. Ellipsometric and resistivity measurements showed a shift from metallic to semiconductor behaviour of the TiO_xN_y films as oxygen flow changed. A solar absorptance value of 0.94 in the solar spectrum region and a low thermal emittance value of 0.05 were achieved for the TiO_xN_y solar absorber coatings prepared at the oxygen partial pressure of $7.5x10^{-5}$ Torr due to both interference and intrinsic absorption. This study confirmed that a single layer of TiO_xN_y film can be a good candidate as selective solar absorber.

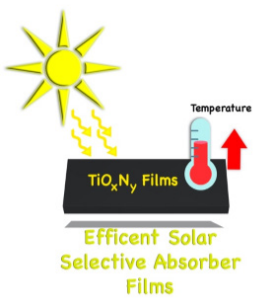

Keywords: Solar Absorber, Tioxny, Oxygen Flow, Structure, Optical Properties

Introduction

The world has an increasing energy demand due to economical and population growth. However, today's energy supply is based primarily on fossil fuels, which are key factors for the majority of greenhouse gas emission and global warming. However, global warming can be reduced by reducing the emission of greenhouse gases and hence there is a need for the improvement of means for using renewable resources. The sun plays a singular role in sustainable energy production, since the supplied energy to Earth in just one hour, exceeds all other renewable energy sources combined. Sun's energy is environmental friendly and can be converted to heat and electricity [1]. Commercially, the solar energy conversion to electricity has been performed through photovoltaic devices based on crystalline, polycrystalline and amorphous silicon. These silicon solar cells represent more than 90% of the world production and the energy conversion mechanism in these devices reach efficiencies in the range of 12-16% and 17-25%, respectively [2]. Another key technology consists of absorbers that convert solar radiation into thermal energy. To harness the abundant solar energy, solar-thermal systems are the most important candidates. An ideal absorber should have high absorbance in UV, visible and near infrared (NIR) regions (0.3 – 2.5 μm) and low thermal emittance in the infrared (IR) region beyond 2.5 μm [3].

The spectrally selective solar absorber surfaces can be designed into different structures including intrinsically selective materials, semiconductor–metal stacks, metal–dielectric stacks, cermet coatings, nanowire arrays, and textured surfaces [4-10]. Of the various designs, due to their high absorption in solar spectral region and the metal volume tunability, the cermet coatings have been widely used [11]. Several cermets based selective solar absorber coatings such as Pt–Al_2O_3, Ag–Al_2O_3, Cu- Al_2O_3, Ni-Al_2O_3, Mo-SiO_2 and W-Al_2O_3, have been reported [12-17]. The cermet consists of small metal particles embedded in a ceramic matrix, where the role of the metallic particles is to increase the solar absorption, due to the interband transitions in the metal, and to reduce the absorption in the thermal IR region due to the small particle size. However, such coatings have limited durability at higher temperature due to oxidation or diffusion of the metal component in the dielectric matrix, which limits their applications [18]. On the other hand, transition metal nitrides and oxynitrides based structures are characterized by a good diffusion barrier, high resistance of oxidation, good mechanical, chemical and thermal properties [19-21]. Several materials such as TiAlN/AlON, W/WSiAlN$_x$/WSiAlO$_y$N$_x$/SiAlO$_x$, TiAlN/TiAlON/SiO_2, and WAlN/WAlON/Al_2O_3 have been reported as selective solar absorbers [22,23].

Recently, an increasing interest has been paid to titanium oxynitride (TiO_xN_y) films due to their interesting properties that make them suitable for a wide range of applications [24]. Depending on the N/O ratios tuneable properties between metallic titanium nitrides and dielectric titanium oxides can be achieved [25]. For instance, TiO_xN_y with low oxygen content have been explored as energy efficient glazing, water-resistant and decorative coatings, transparent infrared window electrodes and components in fuel cell membranes [26-29]. TiO_xN_y materials with high oxygen proportions have been used to produce resistors, insulants, photocatalysis and dye-solar cells [30]. TiO_xN_y have also been investigated as selective solar absorber materials [31,32]. However, the spectral selectivity was achieved by using multi-layer structures and antireflection layers which requires several steps [33-35]. In addition, all the reported TiO_xN_y solar absorber materials have been prepared by using sputtering technique. Single layer TiO_xN_y solar absorber coatings deposited by electron beam evaporation have not been studied yet.

Selective solar absorber coatings prepared by using electron beam (E-beam) evaporation such as Al_xO_y/Pt/Al_xO_y, Cu/Ta/ Al_xO_y/ Pt/Al_xO_y, pure tungsten oxide (WO_3) and iron-doped tungsten oxide (WO_3: Fe), MgO/Zr/MgO and Cu-SiO have been reported [35-39]. These studies showed high solar absorptance in the solar spectrum region and low thermal emittance in the infrared region, which is the basic characteristic of a solar absorber surface. Thus, the aim of this work is to prepare a single layer of TiO_xN_y thin film deposited onto copper, silicon and glass substrates by E-beam evaporation with varying oxygen partial pressures. The effect of oxygen partial pressure on the structural, optical and electrical properties has been investigated.

Experimental details

TiO_xN_y films were deposited onto copper, silicon and glass substrates using an E-beam vacuum evaporation system at room temperature. Before deposition all the substrates were cleaned in an ultrasonic bath and then dried using nitrogen gas blow. The TiO_2 source was placed onto the molybdenum (Mo) liner inside the evaporation vacuum chamber. Samples were deposited by evaporating TiO_2 source at room temperature. Nitrogen and oxygen gases were fed into the chamber and were measured by a mass flow controller. The partial pressure of N_2 gas was optimized and adjusted to $3.6x10^{-5}$ Torr. A beam current of 0.13A was adjusted to attain a deposition rate of 0.8 Å/s. The thickness was optimized and a 110 nm thick film was deposited onto the substrates. Oxygen gas was introduced into the chamber at different partial pressures, namely $7.5x10^{-6}$ Torr, $1.0 x10^{-5}$ Torr, $2.5 x10^{-5}$ Torr and $7.5 x10^{-5}$ Torr. Each TiO_xN_y films was deposited onto copper, silicon and glass substrates in order to characterize the prepared materials in terms of optical performance, morphology, and resistivity of the films.

The crystalline structures of the samples were studied by Model Bruker AXS D8 X-ray diffraction (XRD) system using Cu-K radiation with wavelength of 1.541Å. Elemental analysis was performed using X-ray photoelectron spectroscopy (XPS) spectroscopy. The morphology of the samples was obtained using Leo-Stero Scan 440 scanning electron microscope (SEM). The surface roughness was studied using a Veeco Nanoman atomic force microscope (AFM) V operated in tapping mode. Optical constants and thickness of the films were determined by ellipsometry spectroscopy using Ocean Optics in the wavelength range of 300–2500 nm. The reflectance of the coatings was measured with a Cary 5000 UV–Vis–NIR spectrophotometer from Varian, Inc. (model DRA-2500) in the wavelength range of 300–2500 nm, and with FT-IR spectrophotometer in the wavelength range of 3000-20000 nm. The resistance of the coatings was determined by a sheet resistance meter with four-point probe.

Results and discussion

Microstructure and chemical analysis

Fig. 1 shows x-ray diffraction patterns of TiO_xN_y films deposited on glass substrates with varying oxygen partial pressures. XRD analysis show both crystalline and amorphous structures. All the diffraction patterns revealed that the films exhibited distinct diffraction peaks at 2 =36.86°, 42.760 and 62.26° which correspond to the (111), (200) and (220) orientation of TiN_x phase, and they indicated the existence of crystalline TiO_xN_y. As can be seen from figure 1, the preferred orientation of the films is dependent on the oxygen partial pressure, being (111) at $7.5x10^{-6}$ Torr, (200) at $1.0x10^{-5}$ Torr and $2.5x10^{-5}$ Torr, and (220) at $7.5x10^{-5}$ Torr. This preferred orientation is due to competition between surface energy, strain energy, and stopping energy [40]. The (200), (111) and (220) orientations are dominated by surface energy, strain energy and stopping energy, respectively. These preferred orientations are associated with the N/O composition ratio of the films. This phenomenon has also been observed elsewhere [41]. On the other hand, no diffraction peak associated with TiO_x was detected for all samples, indicating an amorphous morphology of TiO_X at room temperature. This could be due to the fact that when more oxygen content is incorporated into the films, O_2 inhibits the formation of crystallization.

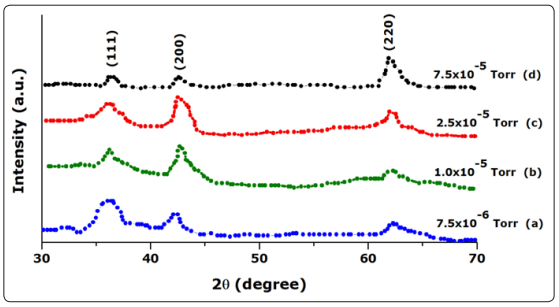

Figure 1: XRD pattern of TiO_xN_y solar absorber coatings for different oxygen partial pressures: $7.5x10^{-6}$ Torr (a), $1.0x10^{-5}$ Torr

(b), 2.5x10^{-5} Torr (c) , and 7.5x10^{-5} Torr (d).

The estimated average crystallite size obtained from Scherer formula for the oxygen partial pressures of 7.5x10^{-6} Torr, 1.0x10^{-5} Torr, 2.5x10^{-5} Torr and 7.5x10^{-5} Torr are 72Å, 75Å, 110Å and 120Å, respectively. It was observed that the crystallite size increases as the oxygen partial pressure increases, which is due to the increase in the density of atoms.

Fig. 2 shows high resolution XPS spectra of TiOxNy thin films deposited onto Si substrates: Ti2p (a), O1s (b) and N1s(c) core-electron spectra by regional scans. The change in chemical states of TiO_xN_y thin films with increasing oxygen partial pressure was studied. As shown in fig.2 (a), the intensity of both $Ti2p_{3/2}$ and $Ti2P_{1/2}$ increases when the partial pressure of oxygen increases from 7.5x10^{-6} to 7.5x10^{-5} Torr, and also a shift towards higher binding energy was observed. This indicates more oxidized state of Ti species than that of TiO_2 due to the incorporation of nitrogen atoms. The increase in Ti atoms with increasing oxygen flux can be due to the connection with O and N atoms [42]. From Fig.2 (b), a decrease in N1s peak with increasing oxygen partial pressure was seen, indicating higher incorporation of oxygen atoms. Moreover an increase in O1s peak intensities as well as a shift towards higher binding energy with increasing oxygen flow was also observed from Fig.2(c).

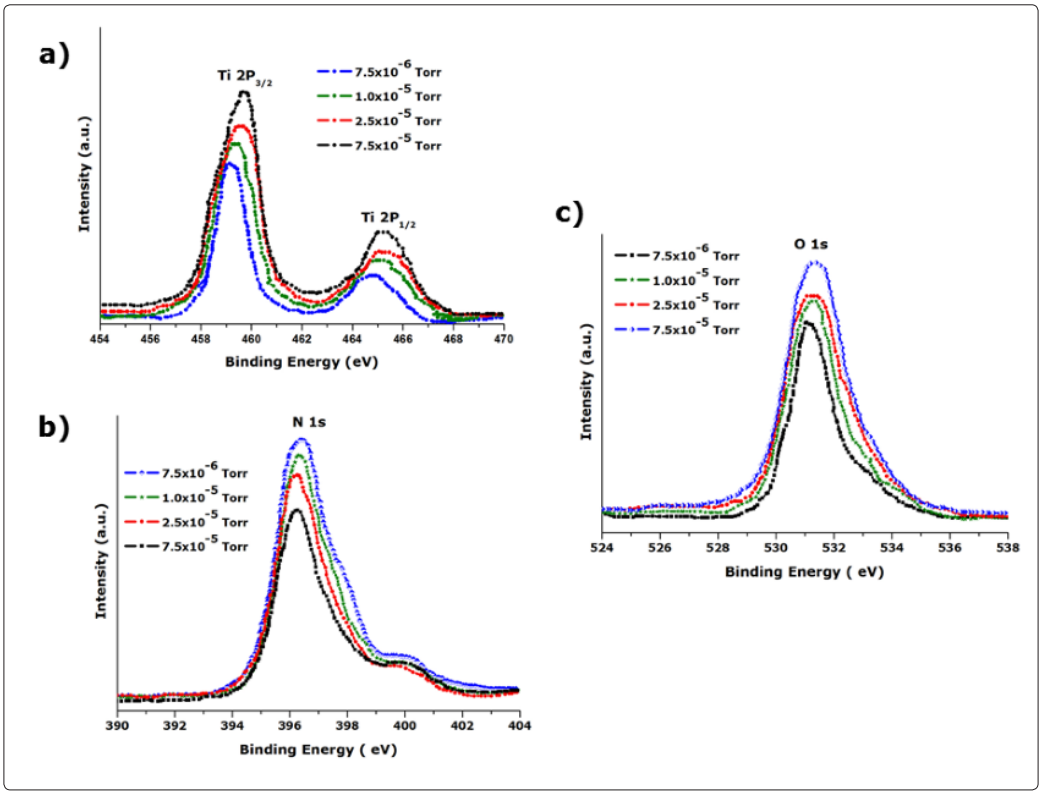

Figure 2: XPS spectra of TiO_xN_y solar absorber coatings for different oxygen partial pressures: Ti2P (a), N1s (b) and O1s (c).

Fig.3 shows SEM micrographs of TiO_xN_y solar absorber coating deposited onto Si substrates at different oxygen partial pressures. At low oxygen partial pressure, the corresponding film exhibits a smooth surface morphology as shown in fig.3 (a). However, with increasing oxygen partial pressure from 7.5x10^{-6} to 1.0x10^{-5} Torr induced formation of randomly distributed spherical like particles are observed as shown in fig.3 (b). By increasing the oxygen partial pressure further to 2.5x10^{-5} and 7.5x10^{-5} Torr uniformly distributed spherical like particles are formed as illustrated in fig. 3(c) & 3(d). The grain size of the TiO_xN_y films increases from 23 to 45 nm as a function of oxygen, which indicates that the growth and structure of the deposited TiO_xN_y thin films are dependent on the oxygen flux.

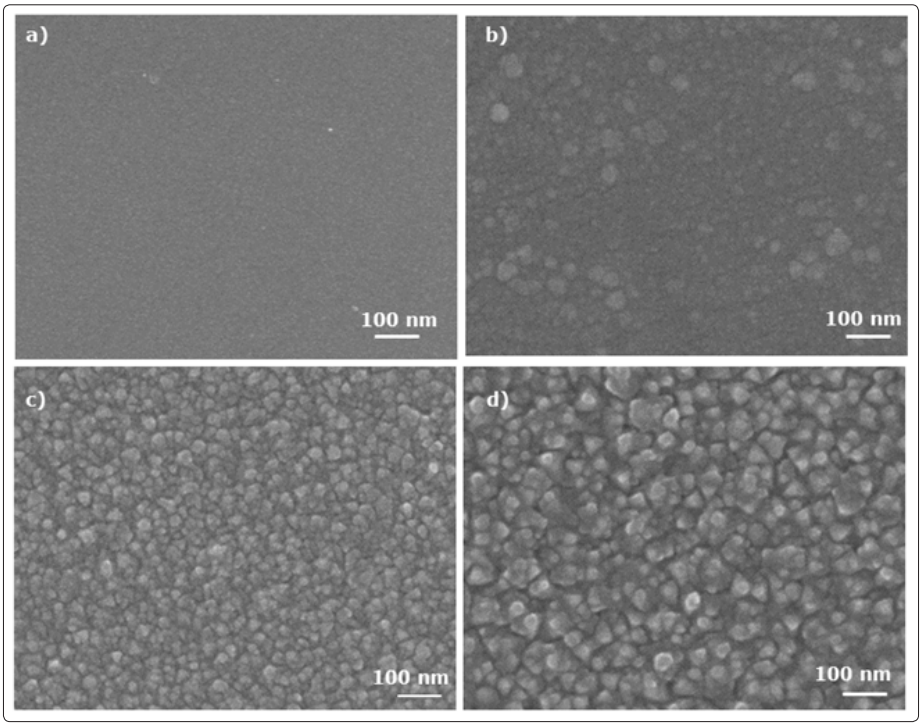

Figure 3: SEM images of TiO_xN_y solar absorber coatings for different oxygen partial pressures: $7.5x10^{-6}$ Torr (a) , $1.0x10^{-5}$ Torr (b), $2.5x10^{-5}$ Torr (c) , and $7.5x10^{-5}$ Torr (d).

Fig.4 shows AFM images of TiO_xN_y solar absorber coatings deposited onto Si substrates at different oxygen partial pressures. The results show that the average surface roughness of the films increases with increasing oxygen partial pressure, confirming the results obtained by SEM. The average surface roughness of TiO_xN_y films increased from 4.8 to 13.8 nm with increasing the oxygen partial pressure, which shows that both grain size and surface roughness can be affected by the oxygen partial pressure. This result also agrees well with the XRD analysis.

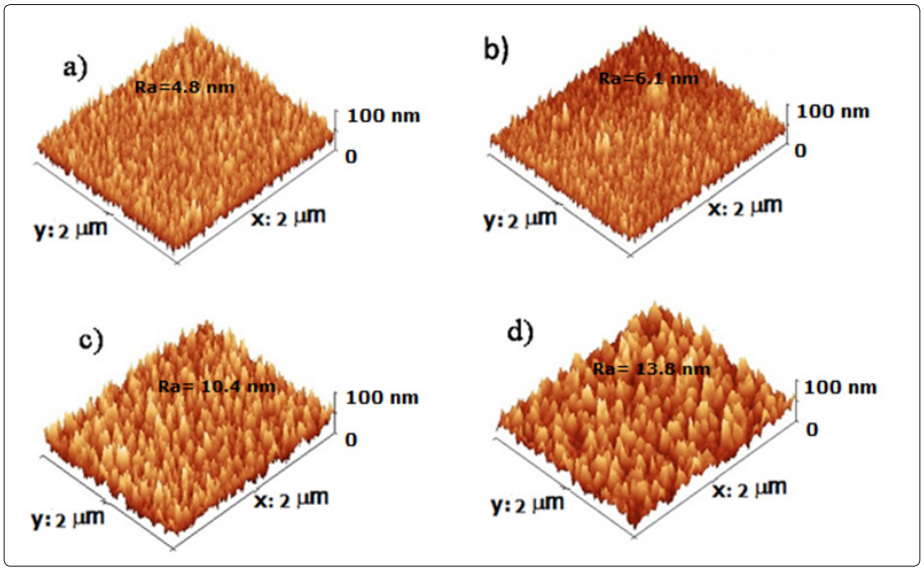

Figure 4: AFM images of TiO_xN_y solar absorber coatings for different oxygen partial pressures: $7.5x10^{-6}$ Torr (a), $1.0x10^{-5}$ Torr (b), $2.5x10^{-5}$ Torr (c) , and $7.5x10^{-5}$ Torr (d).

Optical characterization

The refractive indices and extinction coefficients of TiO_xN_y thin films grown at different oxygen fluxes were estimated from the ellipsometric measurements. Their optical properties are modelled using composite film containing metallic content (TiN) and dielectric component (TiO_2). The free-electron absorption and the localized surface plasmon resonance (LSPR) in TiN can be modelled using Drude model and

Lorenz oscillator. Therefore, the dielectric function of TiO_xN_y (εTiO_xN_y) thin films can be described by the following dispersion model [43].

$$\varepsilon_{TiOxNy} = \varepsilon_\infty - \frac{E_p^2}{E^2 + i\Gamma_D E} + \frac{f_{LSPR}E_{LSPR}^2}{E_{LSPR}^2 - E^2 - i\Gamma_{LSPR}E} + \frac{f_{int}E_{int}^2}{E_{int}^2 - E^2 - i\Gamma_{int}E} \quad (1)$$

where is the high frequency dielectric constant; and are the plasma energy and damping factor of the Drude term contribution of free electron, respectively; and are the strength, resonance energy and damping factor of the LSPR oscillation, respectively; and are the strength, resonance energy and damping factor of the oscillator for the interband transitions, respectively. The obtained optical constants of TiO_xN_y thin films from ellipsometric measurements for different oxygen partial pressures using equation 1 are presented.

Fig. 5 shows the optical constants, refractive index (n) and extinction coefficient (k), of TiO_xN_y thin films deposited onto Si substrates at different oxygen partial pressures (a) $7.5x10^{-6}$ Torr, (b) $1.0x10^{-5}$ Torr, (c) $2.5x10^{-5}$ Torr, and (d) $7.5x10^{-5}$ Torr as a function of wavelength in the range 300-1000 nm. As can be seen from fig. 5(a), n is greater than k in the 300 – 458 nm wavelength range; however, it is smaller beyond 458 nm, which indicates a metallic behaviour. Increasing the oxygen partial pressure to $1.0x10^{-5}$ Torr, and further to $2.5x10^{-5}$ Torr indicates that the value of k is less than that of n beyond 502 and 571 nm, respectively,. This evidences a decrease in metallic behaviour. Moreover, both n and k of these samples (fig.5 (b) and 5(c)) are lower than that of sample grown at $7.5x10^{-6}$ Torr (fig 5(a)), indicating the formation of an oxide due to an increase in oxygen. However, further increase of the oxygen partial pressure to $7.5x10^{-5}$ Torr shows that n is greater than k in most of the solar spectrum region (300 – 1000 nm), demonstrating that light is absorbed in that spectral range. One can also observe that the behaviour of both n and k is almost constant in the long wavelength region, indicating a semiconductor behaviour.

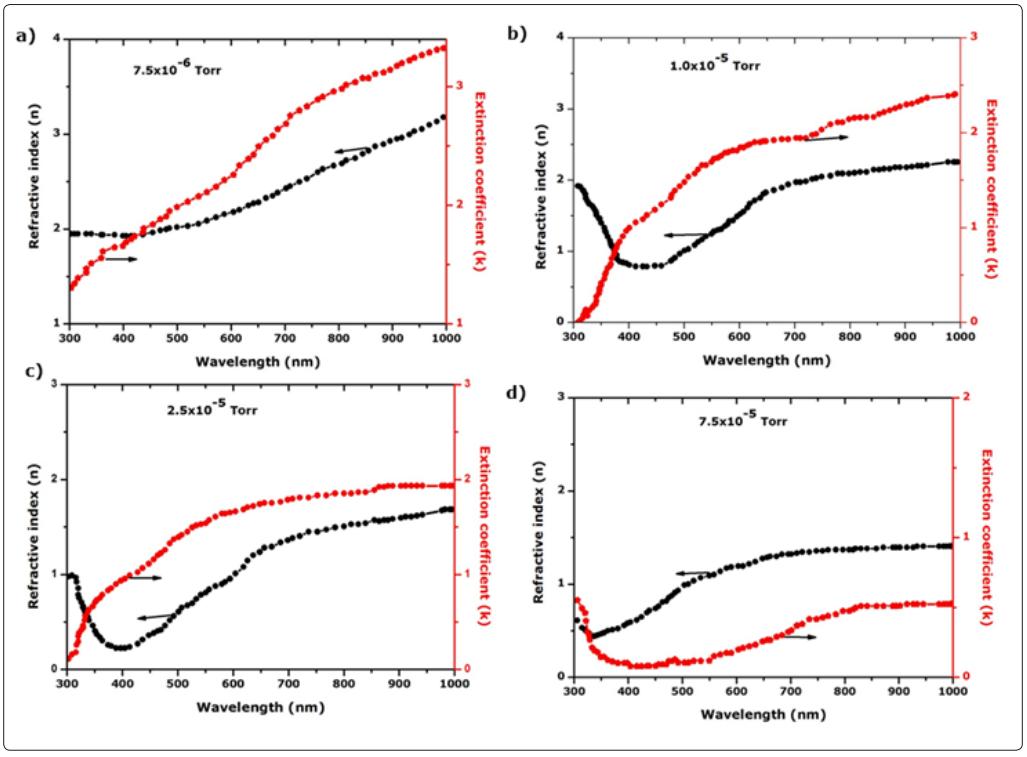

Figure 5: Optical constants of TiO_xN_y solar absorber coatings for different oxygen partial pressures: $7.5x10^{-6}$ Torr (a) , $1.0x10^{-5}$ Torr (b), $2.5x10^{-5}$ Torr (c) , and $7.5x10^{-5}$ Torr (d)

In order to study the basic characteristics of selective solar absorber coating that is solar absorptance and thermal emittance, a reflectance measurement was performed in the UV-Vis-NIR (0.3 – 2.5 μm) and IR region (beyond 2.5 μm). Fig. 6 shows the UV-Vis-NIR spectral reflectance of TiOxNy selective solar absorber coatings for different oxygen partial pressures. The solar absorptance (α) was calculated from the measured reflectance data and weighted by solar irradiance, $I_s(\lambda)$, using standard AM1.5 solar spectrum in the wavelength range of 0.3- 2.5 μm using the following equati

$$\alpha_s(\lambda) = \frac{\int_{0.3\,\mu m}^{2.5\,\mu m} I_s(\lambda)(1 - R(\lambda)d(\lambda)}{\int_{0.3\,\mu m}^{2.5\,\mu m} I_s(\lambda)} \quad (2)$$

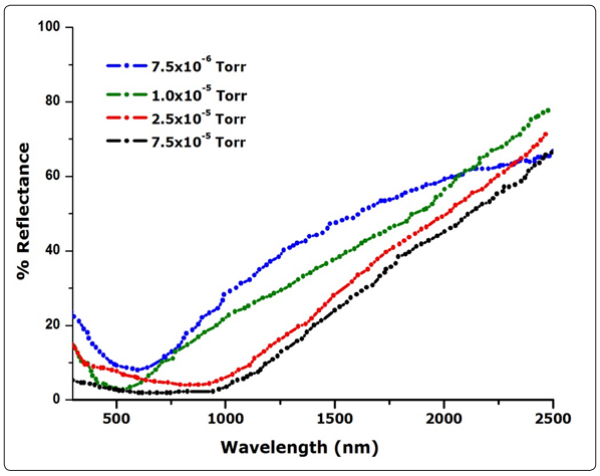

Figure 6: Reflectance spectra of TiO_xN_y solar absorber coatings in the salar spectrum region for different oxygen partial pressures.

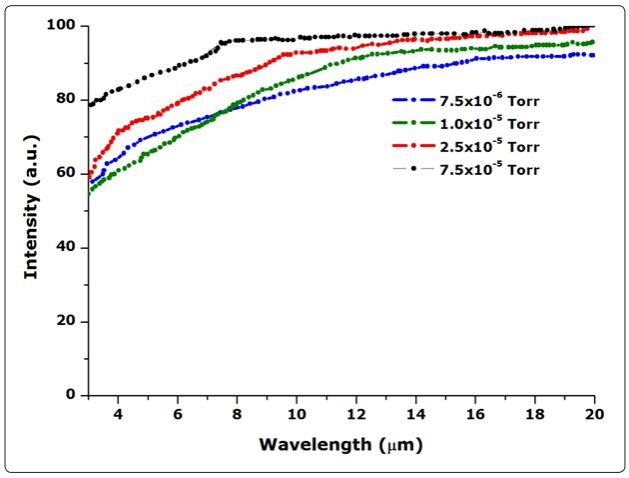

Figure 7: Reflectance spectra of TiO_xN_y solar absorber coatings in the infrared region for different oxygen partial pressures

For the sample prepared at lower oxygen partial pressures of $7.5x10^{-6}$ Torr and $1.0x10^{-5}$ Torr, the cut-off was observed at 640 and 571 nm with 8.2% and 2.4 % reflectance, respectively. Whereas for higher oxygen partial pressures of $2.5x10^{-5}$ and $7.5x10^{-5}$ Torr, the cut-off was at 959 and 963 nm with 5.7% and 2.3% reflectance, respectively. Therefore increasing the oxygen partial pressure shifts the cut-off towards the longest wavelength region, and also a decrease in reflectance in the wavelength range (0.3-0.9) was observed, which induces a high solar absorptance value in the solar spectrum region. The solar absorptance values of the samples are presented in Table 1. A solar absorptance value of 0.94 in the solar spectrum region was obtained for TiO_xN_y thin films with an oxygen partial pressure of 7.5x10-5 Torr, which could be associated with the adequate optical constants as shown by ellipsometric.

Table 1: solar absorptance and thermal emittance values of TiO_xN_y solar absorber coatings grown at various oxygen partial pressures

Partial pressure of oxygen (Torr)	Solar absorptance (α)	Thermal emittance (ε)
$7.5x10^{-6}$	0.84	0.15
$1.0x10^{-5}$	0.87	0.10
$2.5x10^{-5}$	0.91	0.09
$7.5x10^{-5}$	0.94	0.05

In order to verify the thermal radiative property of TiOxNy solar absorber coatings, the reflectance was measured in the infrared region (3 – 20 μm). Fig. 7 illustrates the FT-IR spectral reflectance of TiO_xN_y selective solar absorber coatings for different oxygen partial pressures. The coating prepared at oxygen partial pressure of 7.5x10-6 Torr reflected less than 91% in the infrared region. However, increasing the oxygen partial pressure from $1.0x10^{-5}$ to $7.5x10^{-5}$ Torr caused a slight increase in reflectance and maintained above 90%, which indicates a decrease in thermal emittance of the corresponding coatings.

The thermal emittance was calculated from the measured reflectance data R (λ) and weighted by the blackbody radiation, I_b (λ, T), in the wavelength range of 3 – 20 μm using the following equation:

$$\varepsilon_s(\lambda) = \frac{\int_{3\,\mu m}^{20\,\mu m} I_b(\lambda,T)(1-R(\lambda)d(\lambda)}{\int_{3\,\mu m}^{20\,\mu m} I_b(\lambda,T)} \qquad (3)$$

The calculated thermal emittance of TiO_xN_y solar absorber coatings for different oxygen partial pressures is given in Table 1. It can be seen that the thermal emittance decreased from 0.15 to 0.05 when the oxygen partial pressure is increased. A lower thermal emittance value of 0.05 was calculated for TiO_xN_y coatings with an oxygen partial pressure of $7.5x10^{-5}$ Torr. Hence, amongst the different TiO_xN_y films, the sample with an oxygen partial pressure of $7.5x10^{-5}$ Torr exhibits a good spectral selectivity, i.e. high solar absorptance of 0.94 and low thermal emittance of 0.05, which makes it a good selective solar absorber candidate.

Electrical characterization

To confirm the behaviour of TiO_xN_y films prepared at different oxygen partial pressures, electrical resistivity was measured. Fig. 8 shows the resistivity of TiO_xN_y solar absorber coatings deposited onto glass substrate as a function of oxygen partial pressure. As shown in Fig. 8, the resistivity exhibits a distinctive behaviour with increasing oxygen partial pressure. The resistivity of TiO_xN_y film prepared at the oxygen partial pressure of $7.5x10^{-6}$ Torr was about $3.15x10^{-5}$ Ohm-m, revealing a metallic behaviour. However, when the oxygen flux was increased to corresponding partial pressures of $1.0x10^{-5}$, $2.5x10^{-5}$ and $7.5x10^{-5}$Torr the resistivity of the coatings also increased to 0.0023, 0.0208 and 0.104 Ohm-m, respectively, which indicates a transition to a semiconductor behaviour. Thus, increasing the oxygen partial pressure for the growth of TiO_xN_y coatings shifted the behaviour of the samples from metallic to semiconducting property. This result agrees well with the ellipsometric analysis.

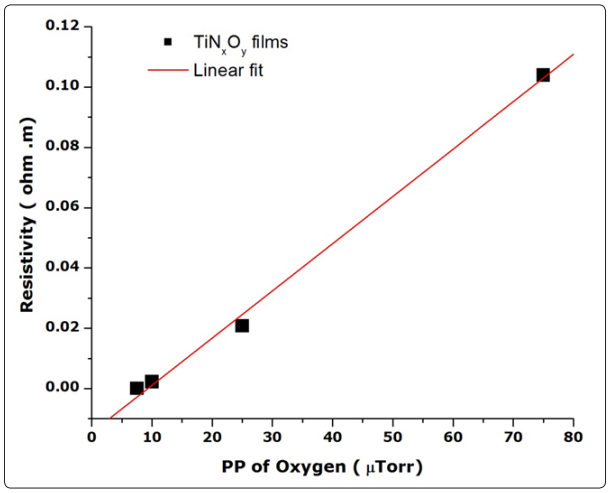

Figure 8: Electrical resistivity of TiO_xN_y solar absorber coatings for different oxygen partial pressures

Conclusion

TiOxNy solar absorber coatings were deposited onto Cu, Si and glass substrates using electron beam evaporation technique at room temperature for different oxygen partial pressures. XRD showed diffraction patterns, which correspond to the (111), (200) and (220) orientation of TiNx phase. The preferred orientation of the films changed as a function of oxygen partial pressure, which is due to the competition between surface energy, strain energy, and stopping energy. XPS showed that the chemical energy states are influenced by the amount of oxygen. The intensity of both Ti $2P_{3/2}$ and Ti $2P_{1/2}$ increases when the partial pressure of oxygen increases, and also a shift towards higher binding energy was observed, indicating more oxidized state of Ti species than that of TiO_2 due to incorporation of nitrogen atoms. SEM demonstrated the formation of uniformly distributed spherical like particles with increasing oxygen partial pressure from $7.5x10^{-6}$ to $1.0x10^{-5}$ Torr. An increase of the average surface roughness of TiO_xN_y films was observed as a function of oxygen partial pressure as depicted from AFM. Ellipsometric measurements have shown that TiO_xN_y films exhibited a metallic behaviour for an oxygen partial pressure of $7.5x10^{-6}$ Torr, and a semiconductor behaviour when the oxygen flux was increased. These properties were also confirmed by resistivity measurements. A solar absorptance value of 0.94 in the solar spectrum region and a low thermal emittance value of 0.05 were achieved for TiO_xN_y solar absorber coatings prepared at the oxygen partial pressure of $7.5x10^{-5}$ Torr. Hence, it can be concluded that this single layer of TiO_xN_y could be a good solar absorber candidate.

Acknowledgements

This work was sponsored by the Future-Leader African Independent Researcher (FLAIR) fellowships in partnership with the African Academy of Sciences (AAS) and the Royal Society, supported by the Global Challenges Research Fund (GCRF).

References

1. Testafamichael T (2000) Characterization of Selective Solar Absorbers.
2. Polman A, Knight M, Garnett EC, Ehrler B & Sinke WC (2016) Photovoltaic materials: Present efficiencies and future challenges. Science 352: aad4424.
3. Nuru ZY, Arendse CJ, Muller TF, Khamlich S & Maaza M (2014) Thermal stability of electron beam evaporated Al_xO_y/Pt/Al_xO_y multilayer solar absorber coatings. Sol Energy Mater Sol Cells 120: 473-480.
4. McDonald GE (1975) Spectral reflectance properties of black chrome for use as a solar selective coating. Sol Energy 17: 119-122.
5. Kats MA, Blanchard R, Genevet P & Capasso F (2013) Nanometre optical coatings based on strong interference effects in highly absorbing media. Nat Mater 12: 20-24.
6. Nuru ZY, Msimanga M, Arendse CJ & Maaza M (2014) Heavy ion elastic recoil detection analysis of AlxOy/Pt/AlxOy multilayer selective solar absorber. Appl Surf Sci 298: 176-181.
7. Karoro A, Nuru ZY, Kotsedi L, Bouziane Kh, Mothudim BM, et al. (2015) Laser nanostructured Co nanocylinders-Al 2 O 3 cermets for enhanced & flexible solar selective absorbers applications. Appl Surf Sci 347: 679-684.
8. Wang Y, Lin Zhou, Qinghui Zheng, Hong Lu, Qiaoqiang Gan, et al. (2017) Spectrally selective solar absorber with sharp and temperature dependent cut-off based on semiconductor nanowire arrays. Appl Phys Lett 110: 201108.
9. Kotsedi L, Nuru ZY, Mthunzi P, Muller TFG, Eaton SM, et al. (2014) Femtosecond laser surface structuring and oxidation of chromium thin coatings: Black chromium. Appl Surf Sci 321: 560-565.
10. Kotsedi L, Nuru ZY, Mthunzi P, Shane Eaton, N. Mongwaketsi, et al. (2015) Femtosecond laser surface structuring of molybdenum thin films. Appl Surf Sci 353: 1334-1341.
11. Bogaerts WF & Lampert CM (1983) Materials for photothermal solar energy conversion. Journal of Materials Science 18: 2847-2875.
12. Teixeira V, Sousa E, Costa MF, Nunes C, Rosa L, et al. (2001) Spectrally selective composite coatings of Cr-Cr_2O_3 and Mo-Al_2O_3 for solar energy applications. Thin Solid Films 392: 320-326.
13. Xiao X, Xu G, Xiong B, Chen D & Miao L (2012) The film thickness dependent thermal stability of Al $_2$O $_3$:Ag thin films as high-temperature solar selective absorbers. J Nanoparticle Res 14: 746.
14. Li Z, Zhao J & Ren L (2012) Aqueous solution-chemical derived Ni-Al $2O_3$ solar selective absorbing coatings. Sol Energy Mater Sol Cells 105: 90-95.
15. Sathiaraj TS, Thangaraj R & Agnihotri OP (1989) $NiAl_2O_3$ cermet solar absorbers by RF planar magnetron sputtering for high temperature applications. Sol Energy Mater 18: 343-356.
16. Zheng L, Fangyuan Gao, Shuxi Zhao, Fuyun Zhou, Jean Pierre Nshimiyimana, et al. (2013) Optical design and co-sputtering preparation of high performance Mo-SiO_2 cermet solar selective absorbing coating. Appl Surf Sci 280: 240-246.
17. Nahar NM, Mo GH & Ignatiev A (1986) A spectrally selective high temperature stable Al_2O_3Co solar absorber coating. Sol Energy Mater 14: 129-141.
18. Selvakumar N & Barshilia HC (2012) Review of physical vapor deposited (PVD) spectrally selective coatings for mid- and high-temperature solar thermal applications. Solar Energy Materials and Solar Cells 98: 1-23.
19. Song P, Yongxin Wu, Lei Wang, Ying Sun, Yuping Ning, et al. (2017) The investigation of thermal stability of Al/NbMoN/NbMoON/SiO_2 solar selective absorbing coating. Sol Energy Mater Sol Cells 171: 253-257.
20. Meng J ping, Liu X peng, Fu Z qiang & Zhang K (2017) Optical design of Cu/Zr0.2AlN0.8/ZrN/AlN/ZrN/AlN/$Al_{34}O_62N_4$ solar

selective absorbing coatings. Sol Energy 146: 430-435.
21. AL-Rjoub, Rebouta L, Costa P, Barradas NP, Alves E, et al. (2018) A design of selective solar absorber for high temperature applications. Sol Energy 172: 177-183.
22. Barshilia HC, Selvakumar N, Rajam KS & Biswas A (2008) Optical properties and thermal stability of TiAlN/AlON tandem absorber prepared by reactive DC/RF magnetron sputtering. Sol Energy Mater Sol Cells 92: 1425-1433.
23. Dan A, Jyothi J, Chattopadhyay K, Barshilia HC & Basu B (2016) Spectrally selective absorber coating of WAlN/WAlON/Al2O3 for solar thermal applications. Sol Energy Mater Sol Cells 157: 716-726.
24. Afzaal M, Yates H & Hodgkinson J (2016) Translation Effects in Fluorine Doped Tin Oxide Thin Film Properties by Atmospheric Pressure Chemical Vapour Deposition. Coatings 6: 43.
25. Vaz, F. Nicolas Martin and Martin Fenker (2013) Metallic Oxynitride Thin Films by Reactive Sputtering and Related Deposition Methods: Process, Properties and Applications. Metallic Oxynitride Thin Films by Reactive Sputtering and Related Deposition Methods: Process, Properties and Applications. Bentham Science Publishers.
26. Warwick MEA, Geoffrey Hyett, Ian Ridley, Fathima R.Laffir, Celia Olivero, et al. (2013) Synthesis and energy modelling studies of titanium oxy-nitride films as energy efficient glazing. Sol Energy Mater Sol Cells 118: 149-156.
27. Chappé JM, Nicolas Martin, Guy Terwagne, Jan Lintymer, Joseph Gavoille, et al. (2003) Water as reactive gas to prepare titanium oxynitride thin films by reactive sputtering. Thin Solid Films 440: 66-73.
28. Jung MJ, Nam KH, Chung YM, Boo JH & Han JG (2003) The physiochemical properties of TiO_xN_y films with controlled oxygen partial pressure. Surf Coatings Technol 171: 71-74.
29. Kim SY, Han DH, Kim JN & Lee JJ (2009) Titanium oxynitride films for a bipolar plate of polymer electrolyte membrane fuel cell prepared by inductively coupled plasma assisted reactive sputtering. J Power Sources 193: 570-574.
30. El-Fattah HA, Mahallawi IEl, Shazly M & Khalifa W (2019) Comparison of Solar-Selective Absorbance Properties of TiN, TiN_xO_y ,and TiO_2 Thin Films. Minerals, Metals and Materials Series 253-263.
31. Eitle J, Oelhafen P, Lazarov MP & Sizmann R (1992) Chemical composition of TiN_xO_y solar selective absorbers in Optical Materials Technology for Energy Efficiency and Solar Energy Conversion XI: Selective Materials, Concentrators and Reflectors, Transparent Insulation and Superwindows (eds. Hugot-Le Goff, A., Granqvist, C.-G. & Lampert, C. M.) 1727: 25-33.
32. Lazarov MP, Brunotte A, Thomas Eisenhammer, Sizmann R, Wolfgang Graf, et al. (1992) Effects of roughness on TiN_xO_y-Cu selective absorbers. in Optical Materials Technology for Energy Efficiency and Solar Energy Conversion XI: Selective Materials, Concentrators and Reflectors, Transparent Insulation and Superwindows (eds. Hugot-Le Goff, A., Granqvist, C.-G. & Lampert, C. M.) 1727: 34-45.
33. Chen F, Wang SW, Yu L, Chen X & Lu W (2014) Control of optical properties of TiN_xO_y films and application for high performance solar selective absorbing coatings. Opt Mater Express 4: 1833-1847.
34. Zhang J, Chen TP, Liu YC, Liu Z & Yang HY (2016) Design of a high performance selective solar absorber with the structure of SiO_2-TiO_2-TiN_xO_y-Cu. ECS J Solid State Sci Technol 5: N43-N47.
35. Zhang J, Chen TP, Liu YC, Liu Z & Yang HY (2017) Modeling of a selective solar absorber thin film structure based on double TiN_xO_y layers for concentrated solar power applications. Sol Energy 142: 33-38.
36. Nuru ZY, Arendse CJ, Khamlich S, Kotsedi L & Maaza MA (2014) Tantalum diffusion barrier layer to improve the thermal stability of Al_xO_y/Pt/Al_xO_y multilayer solar absorber. Sol Energy 107: 89-96.
37. Tesfamichael T, Arita M, Bostrom T & Bell J (2010) Thin film deposition and characterization of pure and iron-doped electron-beam evaporated tungsten oxide for gas sensors. Thin Solid Films 518: 4791-4797.
38. Nuru ZY, Perez D, Kaviyarasu K, Vantomme A & Maaza M (2015) Annealing effect on the optical properties and interdiffusion of MgO/Zr/MgO multilayered selective solar absorber coatings. Sol Energy 120: 123-130.
39. Zhang QC & Mills DR (1992) New cermet film structures with much improved selectivity for solar thermal applications. Appl Phys Lett 60: 545-547.
40. Zhao JP, Xiaohao Wang, Zhi Yu Chen, Yang SQ, Xiaoqing Liu, et al. (1997) Overall energy model for preferred growth of TiN films during filtered arc deposition. J Phys D Appl Phys 30: 5-12.
41. Liou YC & Lu FH (2018) Air-based sputtering deposition of TiN_xO_y films for solar selective absorber coatings applications. Thin Solid Films 660: 733-740.
42. Cho SJ, Jung CK & Boo JH (2012) A study on the characteristics of TiO_xN_y thin films with various nitrogen flow rate by PECVD method. Current Applied Physics 12: S29-S34.
43. Zhang J, Chen TP, Li XD, Liu YC, Liu Y, et al. (2016) Investigation of localized surface plasmon resonance of TiN nanoparticles in TiNxOy thin films. Opt Mater Express 6: 2422-2433.